3D Ion Extraction Code incorporated self-consistently into a numerical Model of a Radio-Frequency Ion Thruster

IEPC-2017-326

Presented at the 35th International Electric Propulsion Conference
Georgia Institute of Technology – Atlanta, Georgia – USA
October 8–12, 2017

Andreas Reeh* and U. Probst†
University of Applied Sciences, Giessen, Hessen, 35390, Germany

Peter J. Klar‡
University of Giessen, Giessen, Hessen, 35392, Germany

Abstract: The grid system is an essential part of a radio-frequency ion thruster (RIT). It determines to a large extent efficiency and lifetime. Existing simulation models for the RIT are able to self consistently predict the thruster's behavior. These models can be used to simulate thruster operating points for different mass flows (through the gas inlet) and ion beam currents. In this paper we propose a more detailed three-dimensional ion extraction model as part of the self-consistent thruster model. Our model yields a simulation of grid currents as well as of the generated thrust. The self-consistent coupling takes into account of how the plasma changes with varying mass flow. We calculated and discussed the influence of beam current and of mass flow on the extraction grids.

Nomenclature

ACG	= acceleration grid
DCG	= deceleration grid
PIC	= particle-in-cell
PB	= plasma boundary
RIT	= radio-frequency ion thruster
RFG	= radio-frequency generator
SB	= space boundary
SCG	= screen grid
THM	= Technische Hochschule Mittelhessen
A	= extraction surface
e	= elementary charge
$\vec{F}_{\mathrm{max}}$	= maximal thrust of the simulation system for a perfect non-divergent extraction
$\vec{F}_{\mathrm{SB}}$	= simulated thrust by particles leaving through the space boundary
i	= discrete address of the potential grid point in x dimension
I_{b}	= beam current, equal to I_{SB}
I_{region}	= current taken by the corresponding region SCG, ACG, DCG or SB

*Research Assistant, Department of Electrical Engineering, andreas.reeh@ei.thm.de
†Professor, Department of Electrical Engineering, uwe.probst@ei.thm.de
‡Professor, Institute of Experimental Physics I, peter.j.klar@exp1.physik.uni-giessen.de

$I_{\mathrm{trajectory}}$	=	current represented by each individual trajectory
j	=	discrete address of the potential grid point in y dimension
k	=	discrete address of the potential grid point in z dimension
k_{b}	=	Boltzmann constant
m_{e}	=	electron mass
m_{i}	=	ion mass
$\dot{m}_{\mathrm{i}}$	=	ion mass flow
$n_{\mathrm{e_s}}$	=	electron sheath density
$n_{\mathrm{i_s}}$	=	ion sheath density
N_{SCG}	=	amount of trajectories which collide with the screen grid
$\vec{p}_{\mathrm{n}}$	=	impulse of a specific particle n
$\vec{p}_{\mathrm{SB}}$	=	impulse by particles leaving through the space boundary
Q_{i}	=	charge of one ion macroparticle
$\vec{r}$	=	position vector
$s_{\mathrm{ACG\_DCG}}$	=	distance between the surfaces from acceleration grid and deceleration grid
$s_{\mathrm{SCG\_ACG}}$	=	distance between the surfaces from screen grid and acceleration grid
t_{gridname}	=	thickness of the corresponding grid
d_{gridname}	=	diameter of the aperture in the corresponding grid
T_{e}	=	electron temperature
T_{i}	=	ion transmission coefficient
v_{b}	=	Bohm velocity
ΔT	=	discrete time step for particle movement
$\triangle x$	=	potential grid distances in x dimension
$\triangle y$	=	potential grid distances in y dimension
$\triangle x$	=	potential grid distances in z dimension
ϵ_0	=	vacuum permittivity
Φ_{region}	=	potential of the corresponding region (PB, SCG, ACG, DCG or SB)
Φ_{s}	=	potential at the electron sheath edge
ρ_{e}	=	electron charge density
ρ_{i}	=	ion charge density
$\rho_{\mathrm{i}}^{\mathrm{n+1}}$	=	ion space charge of iteration n+1 (next iteration)
$\rho_{\mathrm{i}}^{\mathrm{n}}$	=	ion space charge of iteration n (actual iteration)
$\rho_{\mathrm{i}}^{\mathrm{t}}$	=	ion space charge of the trajectories calculated in iteration n
ω	=	under relaxation parameter for the ion space charge

I. Introduction

Radio-Frequency Ion Thrusters rely on separated ionization and extraction mechanisms for generating thrust. This yields a high I_{sp} above 6000 s and thrust scaling over several orders of magnitude. A sketch of the operation principle is shown in Fig. 1. Commercially available thrusters possess nominal thrusts ranging from 50 µN up to 205 mN. Thrust is generated by acceleration of ions by an electrostatic grid system, which, properly adjusted, yields plumes of a small divergence angle. The collisional ionization is powered by inductive heating. For typical thruster-sizes the frequencies of the RF excitation range from slightly below 1 MHz up to a few MHz.

The RIT was invented by Horst Loeb in the 1960s. Since then the technology has been constantly developed and improved by multiple contributors, for example, University of Giessen, ArianeGroup GmbH and Leibniz-Institut fuer Oberflaechenmodifizierung e. V. Since 2012 the Technische Hochschule Mittelhessen (THM) is also involved cooperating with the University of Giessen. The presented work is a further development of our work shown in Ref. 1,2.

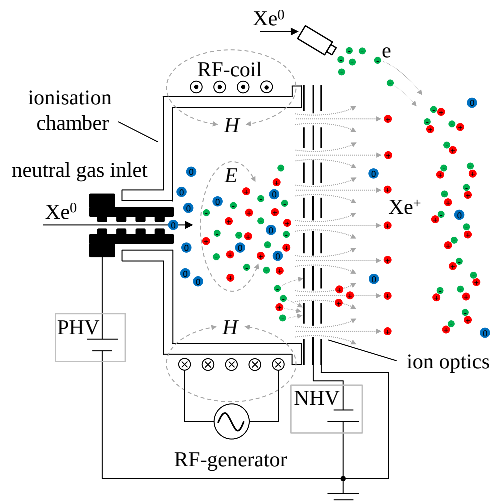

Figure 1. Operation principle of a RIT

One key contribution for further improvements of RIT technology is the ability to model and predict thruster performance with sufficient accuracy. Based on the complexity of the thruster a self-consistent model founded on different areas of physics is required. By running parameter studies the model can be used as a designing tool. Possible parameters are the number of coil windings and distances from coil to housing. For this purpose simulation times in the magnitude of hours are beneficial.

There are two thruster-models[1,2,3,4] which fulfill our requirements for accuracy and simulation time. Both models solve the conservation equations for particles, charge and energy. The second model also calculates the temperature density. For thruster modeling using the models mentioned it is sufficient to calculate the ion mass flow $\dot{m}_\mathrm{i}$ by the expression

$$\dot{m}_\mathrm{i} = v_\mathrm{b} n_{\mathrm{i_s}} A T_\mathrm{i}\left(n_{\mathrm{i_s}}, T_\mathrm{e}, \Phi_\mathrm{SCG}, \Phi_\mathrm{ACG}, \Phi_\mathrm{DCG}\right) \tag{1}$$

where v_b is the Bohm velocity, $n_{\mathrm{i_s}}$ is the ion sheath edge density and A is the extraction surface. The grid system is described by an ion transmission coefficient T_i dependent on ion sheath edge density, electron temperatur T_e, and the grid potentials Φ_SCG, Φ_ACG and Φ_DCG as indicated in Fig. 2. Equation (1) is used as part of the particle conservation.

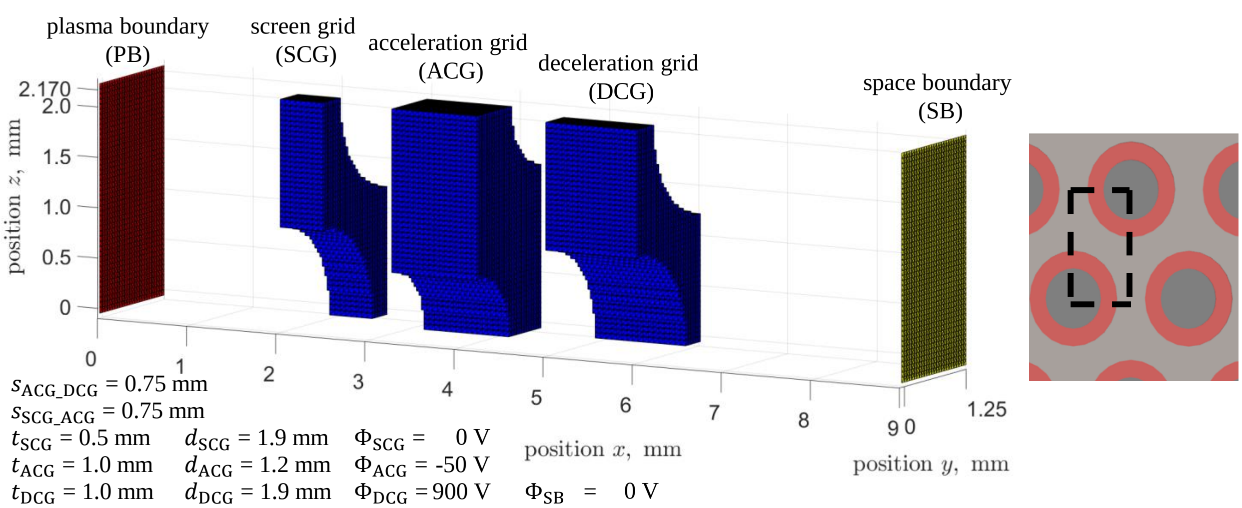

Figure 2. Ion optics of a RIM-4 as represented in our extraction model with boundary conditions

The grids' purpose is to accelerate ions for thrust generation and also to keep the neutral gas inside the ionization chamber. For good efficiency the ion transmission coefficient has to be high and the neutral gas transparency has to be low. This leads to a design where the ion flux out of the plasma is focused from a wide aperture in the screen grid through a narrow aperture in the acceleration grid. Based on the plasma parameters n_{i_s} and T_e as well as the grid geometry and the grid potentials different effects can be observed[5,6,7]. E.g.:

a) direct impingement

b) cross-over

c) electron back streaming

d) thrust reduction by divergence

e) widening of the plasma meniscus inside of the plasma

In Ref. 3 and 4 the ion extraction software IBSimu with a 2D axisymmetric ion optics geometry was used. The software simulates the ion beam which includes a)-e) but only the ion transmission coefficient and the divergence are evaluated. To the author's knowledge, there is no self-consistent thruster model for an RIT which evaluates a)-d). For this purpose, we propose to improve our previously developed model of a RIT[1,2] by including a more sophisticated three-dimensional ion extraction code. In addition, we evaluate how the operating point of the grids changes dependent on the beam current and on the amount of incoming neutral gas.

II. Numerical Model

A. Thruster model

The thruster is modeled according to Ref. 1-5 and 8-13. As the focus of this paper is on the ion extraction, we will just give a short overview of the thruster model. Three conservation equations for energy, charge and particle number are used. The self-consistent model calculates electron temperature, ion density and neutral gas pressure inside the ionization chamber. The energy conservation ensures that the lost power inside the plasma equals the induced power by the coil. Within this model the quasi stationary electromagnetic field equations are solved using the finite difference method. The charge conservation balances generated charge by ionization and lost charge at the walls and by extraction. The particle conservation takes into account the incoming neutral gas (abbreviated as mass flow), the lost neutrals through the grids as well as the extracted ions. To calculate the number of extracted ions the new extraction code is used.

B. Ion extraction model

The simulation of ion extraction is already well known and validated. Thus, many simulation tools e.g. IGUN[10], Kobra and IBSimu[11,12] are available and act as reference. There are models for 2D and 3D simulation. As seen in Fig. 2, our code simulates ion optics in 3D. In y and z direction the Neumann boundary condition are applied for the potential calculation and particles are mirrored. At PB and SB Dirichlet boundary condition are applied and particles are deleted. As illustrated on the right-hand side of Fig. 2 the simulated region represents one unit cell of an unlimited number of apertures in a hexagonal layout. This allows us to evaluate the effects of neighboring extraction apertures[13].

C. Simulation domain and Particle-in-Cell method

For ion simulation, the particle-in-cell (PIC) method is used[14,15]. As shown in Fig. 3, the whole simulation domain is divided into voxels/cells. The voxel edges are used as a grid system for the electrostatic potential. The ions are represented by macroparticles. If a macroparticle leaves a cell, it will be checked whether it collides in the neighboring cell. The parameters assigned to the neighboring voxel define the applied behavior:

a) no action (vacuum)

b) deletion of macroparticle (material)

c) reflection of macroparticle (boundary to neighboring aperatures)

By representing the hexagon layout as shown in Fig. 2 the size of the simulation domain is determined by the distance between two aperture centers. This necessitates to choose the voxel length x, y and z independently. The PIC method requires the particle charge to be assigned to the grids (scatter) and the electric field calculated from the potential to be interpolated to the particle position (gather). In our code we apply a first order weighting for both scatter and gather. To integrate the equation of motion (move) the Boris scheme[15] comes into effect. For performance enhancement gather and move are executed in parallel on several cores using multithreading. The C++ Standard Library is used for programming.

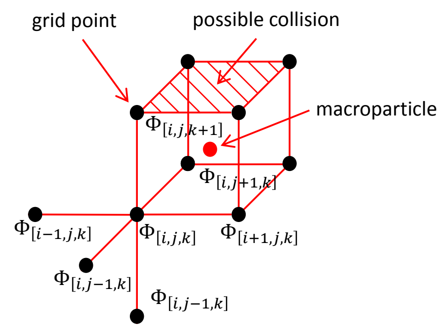

Figure 3. Voxel representation and grid system for the electrostatic potential

D. Flow Chart

A Vlasov-Poisson iteration[13] as shown in Fig. 4 is used to solve the system until convergence. The electrostatic potential is calculated during each iteration. Based on the newly calculated potential the ion macroparticles are moved discrete time steps starting at predefined starting positions. This is done until every particle is either deleted due to a collision with grid material or has moved outside the simulation domain by reaching the space boundary. In order to determine convergence, a norm for the positional deviation between iteration n and iteration $n+1$ is calculated. Convergence is assumed when the norm is smaller than a given value. If the convergence is not reached, the under relaxation method is used to calculated the ion space charge for the next iteration ρ_i^{n+1} by

$$\rho_\mathrm{i}^{n+1} = \rho_\mathrm{i}^{n} + \omega\big(\rho_\mathrm{i}^{t} - \rho_\mathrm{i}^{n}\big) \tag{2}$$

where ρ_i^{n} is the actual ion space charge used for trajectory calculation, ω is the under relaxation parameter and ρ_i^{t} is the ion space charge of the calculated trajectories of iteration n. This process is repeated until the convergence criteria is met.

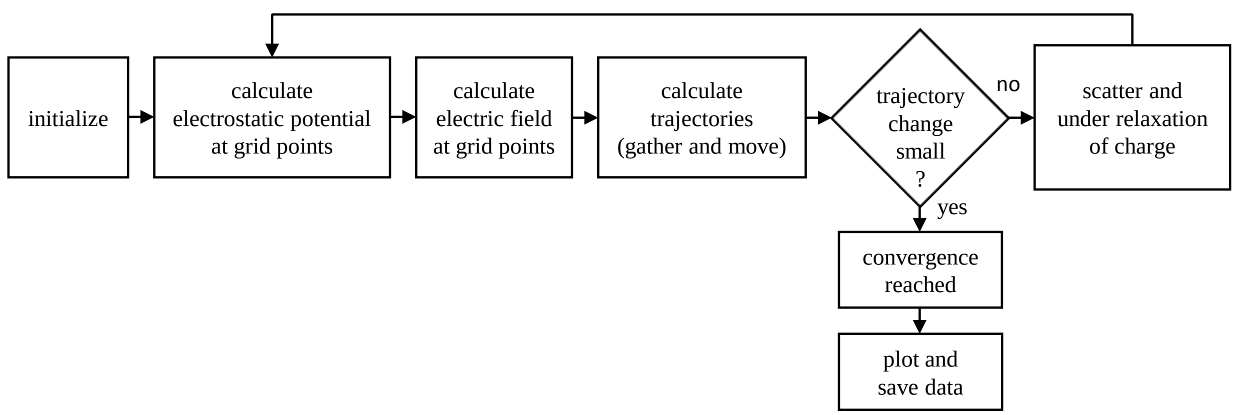

Figure 4. Flow chart of the used Vlasov-Poisson iteration

E. Boundary conditions

The ion trajectories start near the plasma boundary. A collisionless sheath is assumed. We use the Bohm velocity

$$v_\mathrm{b} = \sqrt{\frac{k_\mathrm{b} T_\mathrm{e}}{m_\mathrm{i}}} \tag{3}$$

as start velocity for the ions, where k_b is the Boltzmann constant and m_i is the ion mass. The thruster model provides the electron temperature and the ion sheath edge density.

We apply a Dirichlet boundary condition at the boundary of both space and plasma. The potential at the space boundary is 0 V. To calculate the Φ_PB at the plasma boundary we use the well known equation for the sheath potential. We calculate

$$\Phi_\mathrm{PB} = \Phi_\mathrm{ACG} + \frac{k_\mathrm{B} T_\mathrm{e}}{2e} \ln\left(\frac{m_\mathrm{i}}{2\pi m_\mathrm{e}}\right), \tag{4}$$

where e is the elementary charge and m_e is the electron mass.

To model the plasma sheath a distance of at least 20 Debye lengths is simulated between plasma boundary and screen grid. The voxel length in x direction and thus the distance of the potential grid points is below one Debye length. The ion macroparticle charge Q_i is calculated by

$$Q_\mathrm{i} = \frac{I_\mathrm{trajectory}}{\Delta T} \tag{5}$$

where $I_\mathrm{trajectory}$ is the current per trajectory and ΔT is the discrete time step for particle movement. This calculation ensures that the trajectories correctly represent the space charge. The electron sheath density $n_{\mathrm{e_s}}$ is assumed to be equal to the ion sheath density $n_{\mathrm{i_s}}$.

F. Nonlinear Poisson equation

The potential is described by the Poisson equation

$$\nabla^2 \Phi = -\frac{\rho_\mathrm{i} + \rho_\mathrm{e}}{\epsilon_0} \tag{6}$$

where ρ_e is the electron charge density, ρ_i is the ion charge density and ϵ_0 is the vacuum permittivity. The ion charge density is defined by the ion macroparticles. The electron density is assumed to follow the Boltzmann relation[17]. This leads to the analytical equation

$$\rho_\mathrm{e}(\vec{r}) = -e n_{\mathrm{e_s}} \exp\left[\frac{e}{k_\mathrm{B} T_\mathrm{e}} \left(\Phi(\vec{r}) - \Phi_\mathrm{s}\right)\right] \tag{7}$$

where $\vec{r}$ is the position vector and Φ_s is the potential at the electron sheath edge. A discretization is needed to solve the partial differential equation by numerical methods. In this work the finite difference method is applied to Eq. 6 and 7 leading to the following 7-point stencil:

$$\begin{aligned}
D_x + D_y + D_z &= -\frac{\rho_\mathrm{i} - e n_{\mathrm{e_s}} \exp\left[\frac{e}{k_\mathrm{B} T_\mathrm{e}} \left(\Phi_{[\mathrm{i,j,k}]} - \Phi_\mathrm{s}\right)\right]}{\epsilon_0} \\
D_x &= \frac{\Phi_{[\mathrm{i-1,j,k}]} - 2\Phi_{[\mathrm{i,j,k}]} + \Phi_{[\mathrm{i+1,j,k}]}}{(\triangle x)^2} \\
D_y &= \frac{\Phi_{[\mathrm{i,j-1,k}]} - 2\Phi_{[\mathrm{i,j,k}]} + \Phi_{[\mathrm{i,j+1,k}]}}{(\triangle y)^2} \\
D_y &= \frac{\Phi_{[\mathrm{i,j,k-1}]} - 2\Phi_{[\mathrm{i,j,k}]} + \Phi_{[\mathrm{i,j,k+1}]}}{(\triangle z)^2}
\end{aligned} \tag{8}$$

where i,j and k are the discrete addresses of the potential grid points in x,y and z direction as shown in Fig. 3 and $\triangle x$, $\triangle y$ and $\triangle x$ are the potential grid distances.

Particular consideration must be given to Dirichlet and Neumann boundary conditions. Dirichlet boundary conditions can be applied at any potential grid point. Neumann boundary conditions can only be used at outer potential grid points of the simulation domain. If necessary, we apply different equations for 6 surfaces, 8 corners and 12 edges respectively. The nonlinear equation is solved by using a multidimensional Newton-Raphson method. In this method, a linear system of equations is generated based on an initial potential. The solution of this linear system of equations is used as a correction to the potential. This is repeated until convergence is met. The linear system of equations is solved using Red-Black-SOR[18]. For performance enhancement this algorithm is executed in parallel on several cores using multithreading. The C++ Standard Library is used for programming.

G. Characterization of a grid operating point

For grid characterization, the previously introduced effects a)-d) (see Introduction) have to be quantified. This is done on the basis of the following assignments:

- current to ACG and DCG $\rightarrow$ indication for crossover and direct impingement
- current to space boundary $\rightarrow$ ion transmission coefficient
- force to space-boundary $\rightarrow$ thrust and indication for defocusing
- lowest potential inside the beamlet $\rightarrow$ indication for electron backstreaming

To determine the values, each voxel is assigned to a region. These regions are SCG, ACG, DCG, and SB as shown in Fig. 2. For each region we record the ion current occurring and the force exerted on the region. Each trajectory represents a fraction of the ion current leaving the plasma. The ion current assigned to a specific region is calculated by summing up all the ions which imping on these region. E.g. the ion current I_{ACG} assigned to the acceleration grid is calculated by

$$I_{\mathrm{ACG}} = N_{\mathrm{ACG}} I_{\mathrm{trajectory}} \tag{9}$$

where N_{ACG} is the amount trajectories which impinge on the acceleration grid. Other ion beam currents are calculated accordingly.

Each macroparticle carries a momentum. The amount of particles which collide with the space boundary in the trajectory calculation corresponds to with the collisions which take place every time step ΔT. As an illustration: Each time step every particle jumps to the next trajectory position. Accordingly each time step the amount of particles generated at the start of the trajectories corresponds to the amount of deleted particles at the end of the trajectories. By summing up the momentum of all particles which collide with the SB in the trajectory calculation we also obtain the total momentum which leaves the system every time step ΔT. Thus, the thrust $\vec{F}_{\mathrm{SB}}$ is calculated by

$$\vec{F}_{\mathrm{SB}} = \frac{\partial \vec{p}_{\mathrm{SB}}}{\partial t} \approx \frac{\sum\limits_{n \in SB} \vec{p}_{\mathrm{n}}}{\Delta T} \tag{10}$$

where $\vec{p}_{\mathrm{SB}}$ is the total momentum of all ions, that leave the SB per time interval, $\vec{p}_{\mathrm{n}}$ is the momentum vector of a specific macroparticle n and $\sum_{n \in SB}$ is the summing over all macroparticles, that hit the space boundary.

The result agrees with the sum of momentum generated from the electric field by acceleration and the one based on the Bohm velocity. We assume, that the force outside the simulation area is negligible. This assumption corresponds to applying a Dirichlet boundary of 0 V at the space boundary.

H. Validation of the implementation

Our code is based on physical assumptions identical to those of already existing and validated ion extraction codes. Accordingly, the validation of the equation system can be omitted and it is sufficient to validate the correct implementation. This is done by comparing the trajectories of our code with the trajectories from IGUN as shown in the left part of Fig. 5. In IGUN a 2D axisymmetric system is simulated with a radius of 1.41 mm. In our 3D-Code we simulate a rectangular system with the holes in the middle and periodic boundaries towards the neighbor-holes as shown on the right-hand side of Fig. 5. The area in our code of $2.5 \cdot 2.5$ mm^2 is chose such as to simulate the same sheath surface and thus, also the same beam current as in IGUN. The system length in both cases is 12 mm. As aperture we use our RIM-4 configuration already shown in Fig. 2. The electron temperature and the ion-starting energy are set to 3.0 eV. As depicted in the left part of Fig. 5 a good agreement is achieved.

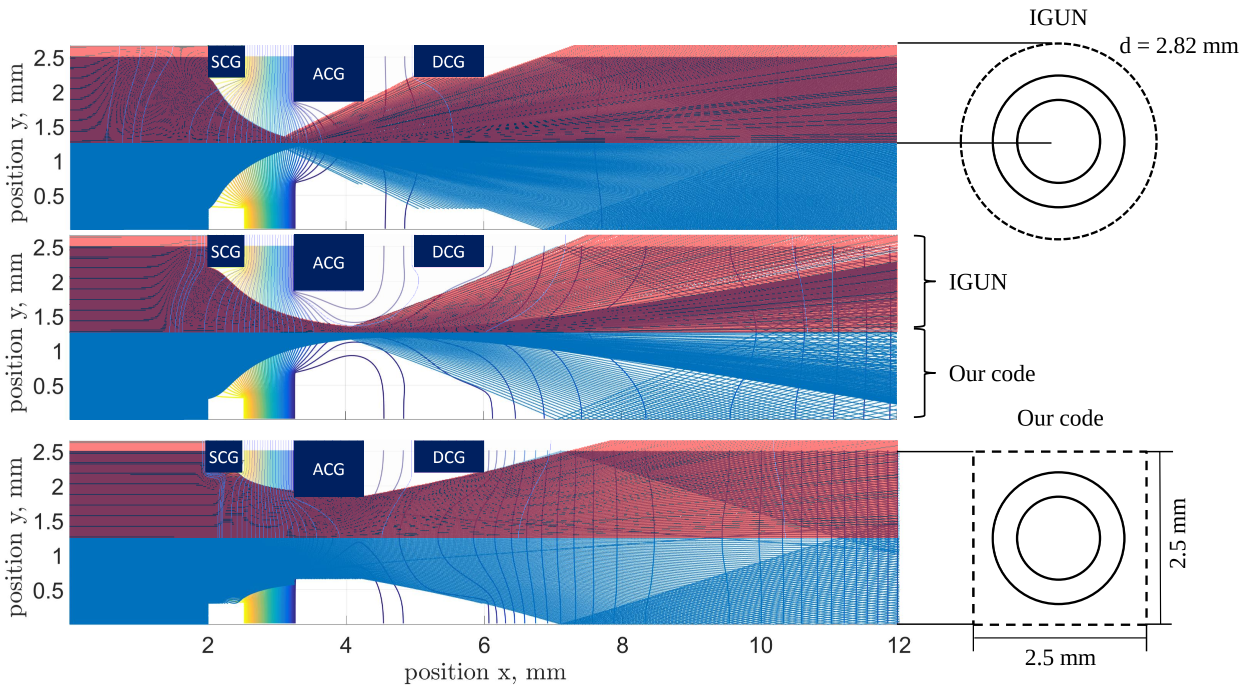

Figure 5. left: Validation of our extraction code with IGUN for ion density $10^{15}\frac{\#}{\mathrm{m}^3}$ (top), $10^{16}\frac{\#}{\mathrm{m}^3}$ (middle) and $10^{17}\frac{\#}{\mathrm{m}^3}$ (bottom); right: sideview of simulation domains

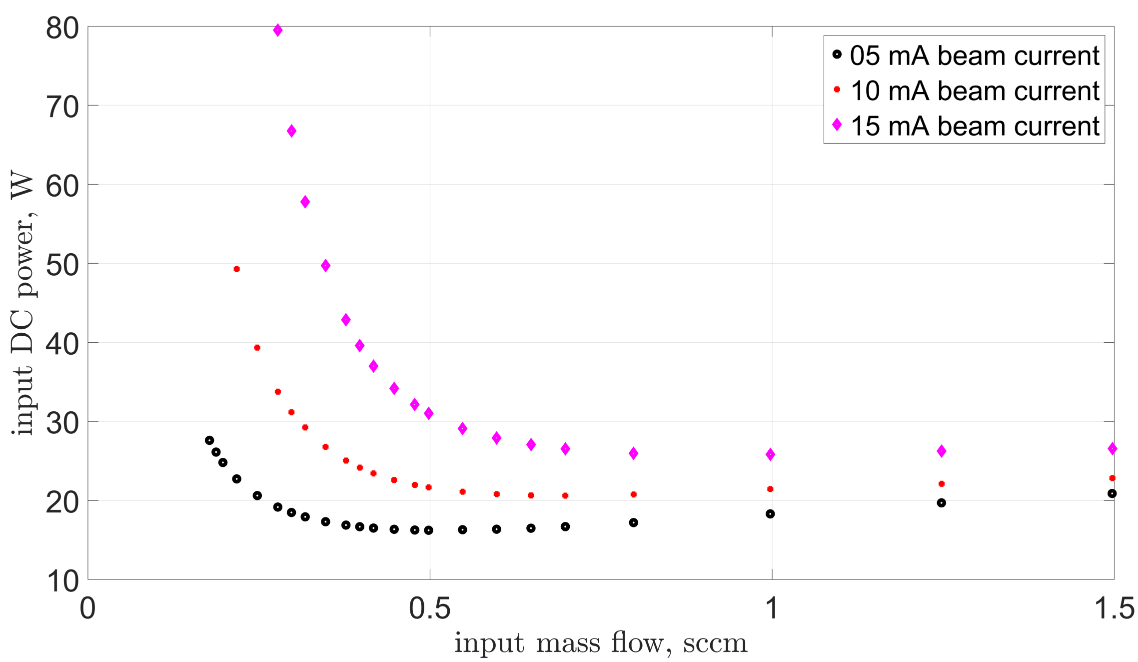

Figure 6. Measured performance mapping of the RIM-4 at 2 MHz excitation frequency and different beam currents

III. Results

A. Performance Mapping

To evaluate a RIT a performance mapping as depicted in Fig. 6 is measured.

The thruster model combined with the extraction model allows us to calculate the ion sheath edge density as well as the electron temperature for different thruster operating points as depicted in Fig. 7. A thruster operating point is defined by the input mass flow $\dot{m}_{\mathrm{in}}$ of the neutral gas and the ion beam current I_{b}. In the following all simulations are done for our RIM-4 and at a excitation frequency of 2 MHz.

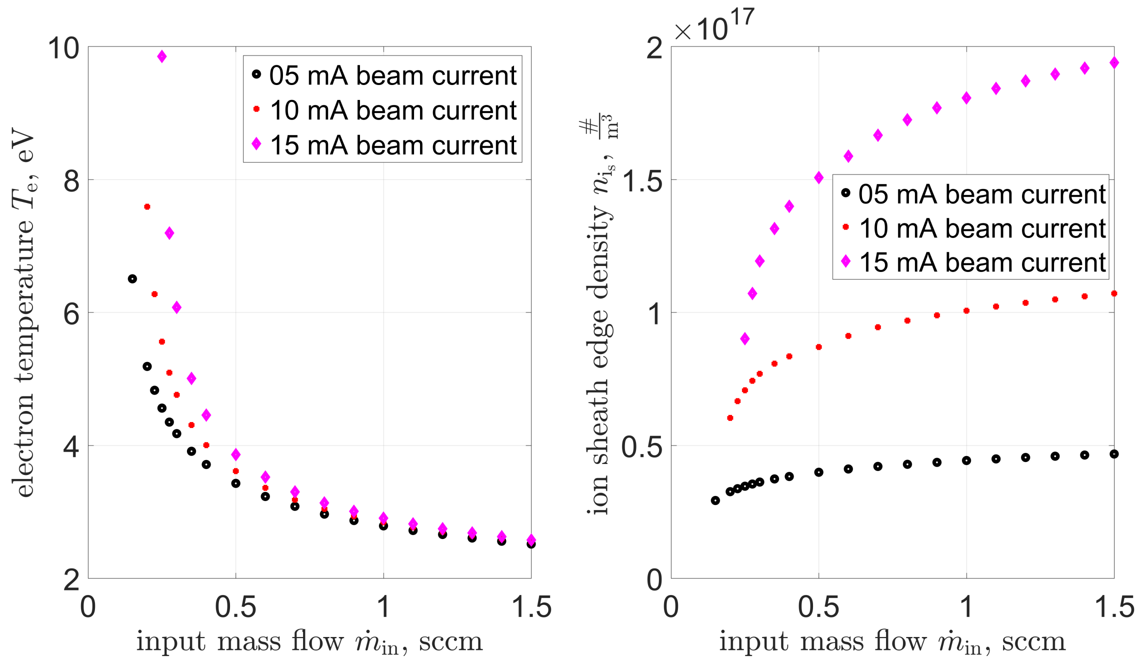

Figure 7. Calculated electron temperature and ion sheath edge density for RIM-4 at 2 MHz excitation frequency

B. Ion optics characterization

We analyzed the behavior of the ion optics for different thruster operating points. To do this, we ran 300 simulations for different ion sheath densities and electron temperatures in our 3D code. This took 60 hours of simulation time. In x, y and z direction the potential for 130 to 693, 44 and 26 grid points were solved. In every simulation 18304 trajectories were calculated. The electron temperature was varied between 1.0 eV and 20 eV in 15 steps. The ion sheath density was varied between 10^{16} $\frac{\#}{\mathrm{m}^3}$ and 10^{18} $\frac{\#}{\mathrm{m}^3}$ in 20 steps. The intervals for both parameters were stepped logarithmically. In Fig. 8 trajectories for four combination possibilities of min and max values of T_{e} and $n_{\mathrm{i_s}}$ are illustrated. This figure can be used to explain the basic behavior of the ion optic.

According to Eq. (3) a low electron temperature leads to a low starting velocity. Additionally the sheath potential (see Eq. (10)) is also low which leads to less acceleration of the ions in the sheath. The overall lower velocity allows the ions to be diverted more easily. This can be seen by comparing top left and bottom left images of Fig. 8.

At low ion sheath density (left in Fig. 8) and low electron temperature (bottom in Fig. 8) the trajectories are pulled towards the middle of the aperture, before they reach the screen grid. Therefore, more ions can pass through the screen aperture and I_{SCG} is reduced. This combination of T_{e} and $n_{\mathrm{i_s}}$ also leads to a plasma meniscus (equipotential for $\Phi = \Phi_{\mathrm{ACG}}$) which penetrates far into the plasma. The diversion can be large enough to let the ions cross the center of the aperture and impinge on the grid at the opposite side. This is called cross-over.

At low ion sheath density (left in Fig. 8) and high electron temperature (top in Fig. 8) the ion divertion between space boundary and screen grid is negligible. The ions approach the screen grid approximately

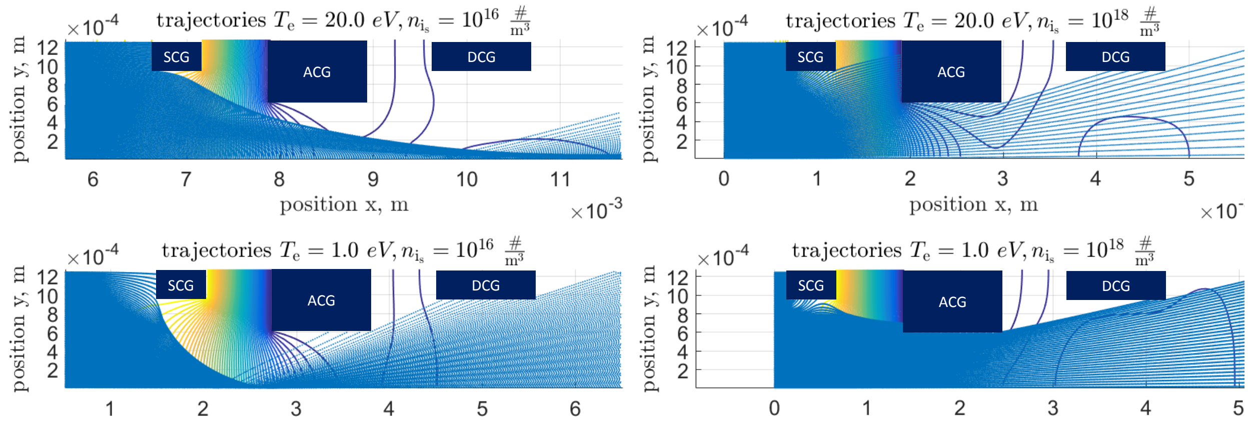

Figure 8. Trajectories for different values of T_e and n_{i_s}

perpendicular to its surface. The extracted current is determined by the geometrical area ratio between screen grid aperture and simulation domain. The ratio is approximately 0.52 which coincides with the value in Fig. 9.

At high ion sheath density (right in Fig. 8) the grid operating points move towards the perveance limit. The ion space charge lets the beamlet expand. This leads to additional ion current towards the screen grid at the inside of the aperture. Furthermore, accelerated ions hit the acceleration grid. This leads to so called direct-impingement.

C. Screen grid current

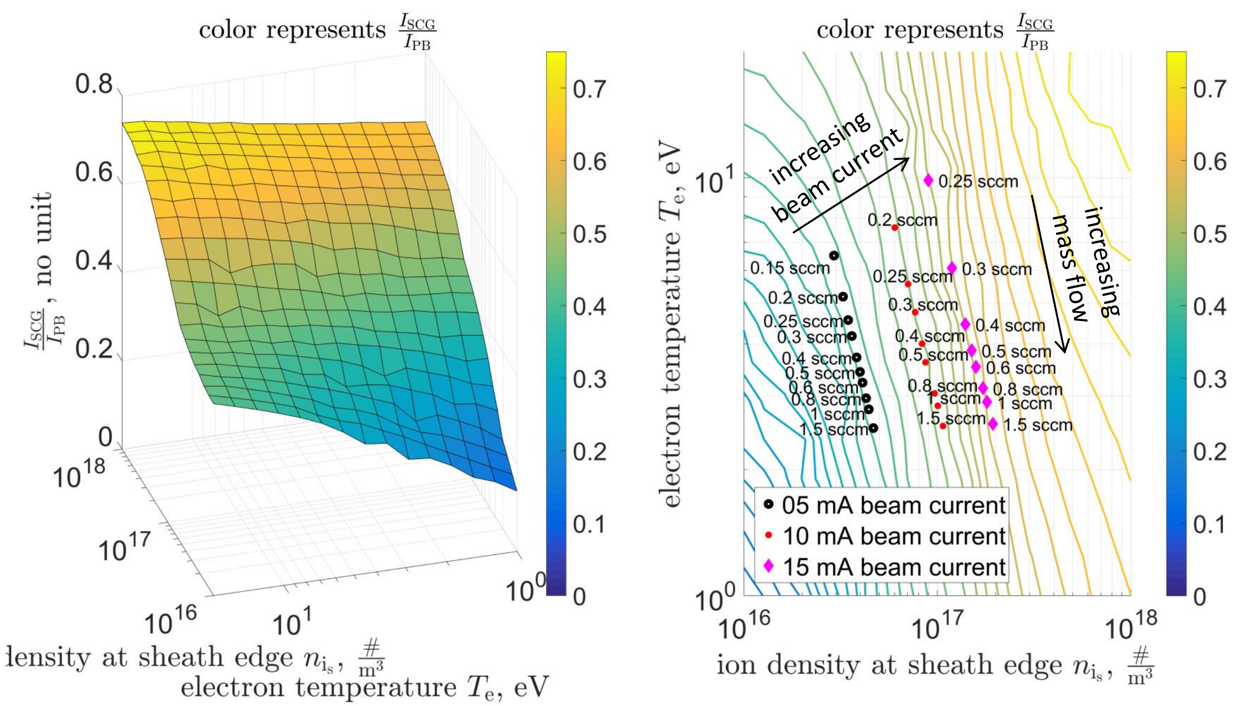

Figure 9. current ratio towards screen grid, left: surface plot; right: lines of constant ratio with the operating points from Fig. 7. Positions from bottom to top represent the input mass flow from high to low.

In Fig. 9, we analyze the screen grid current I_{SCG}. All grid currents are divided by the total ion current out of the plasma boundary I_{PB}. This leads to a value range from 0 to 1. As depicted on the left-hand side of Fig. 7 this proportion changes from roughly 0.2 up to 0.7. These values are in accordance with the trajectories shown in Fig. 8.

The right-hand image of Fig. 7 shows lines of constant ratio $\frac{I_{\mathrm{SCG}}}{I_{\mathrm{PB}}}$ together with the operating points of the thruster. For the operating points the same values as in Fig. 7 are used. With increasing input mass flow the neutral gas density inside the ionization chamber will also increase. A higher neutral gas density leads to a lower electron temperature. As a consequence the Bohm velocity decreases. Due to current control the ion beam current is constant. Based on Eq. (1) the decreased Bohm velocity is compensated by the controller with an increase in the ion density. This dependence is displayed in Fig. 9.

It may be expected that this affects the aperture operating point. As seen in Fig. 9 the decreasing electron temperature and the increasing ion density seem to counteract each other. By varying the input mass flow the operating point of the aperture changes along the lines of constant ratio. This effect will be shown later again for the other parameters.

A change of beam current leads to a change perpendicular to the lines of constant ratio $\frac{I_{\mathrm{SCG}}}{I_{\mathrm{PB}}}$. This changes the operating point.

D. Acceleration and deceleration grid current

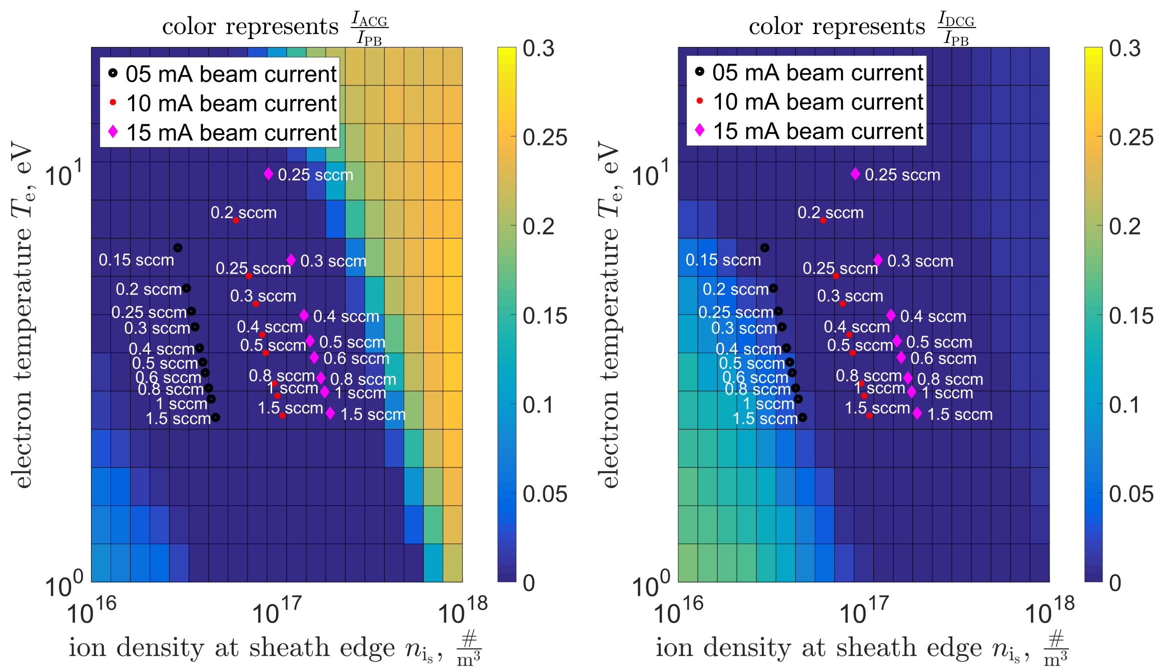

Figure 10. left: current ration towards acceleration grid; right: current ration towards deceleration grid

Next we evaluate the grid currents. The top right region in both images of Fig. 10 indicates direct impingement. The bottom left corner indicates crossover. Both effects result in currents to both grids with different magnitude:

Direct impingement → strong acceleration grid current, minor deceleration grid current.
Crossover → strong deceleration grid current, minor acceleration grid current.

Both grid currents lead to the unwanted effect of grid erosion. In Fig. 11 the sum of acceleration grid current and deceleration current is illustrated. A corridor (blue) for possible operating points without grid erosion can be seen. Grid erosion by charge exchange ions is not considered.

- Varying the inlet mass flow → grid operating point changes along the corridor.
- Varying the beam current → grid operating point changes perpendicular to the corridor.

When the region of direct impingment is reached, the gradient is quite strong which leads to a fast rise of acceleration grid current.

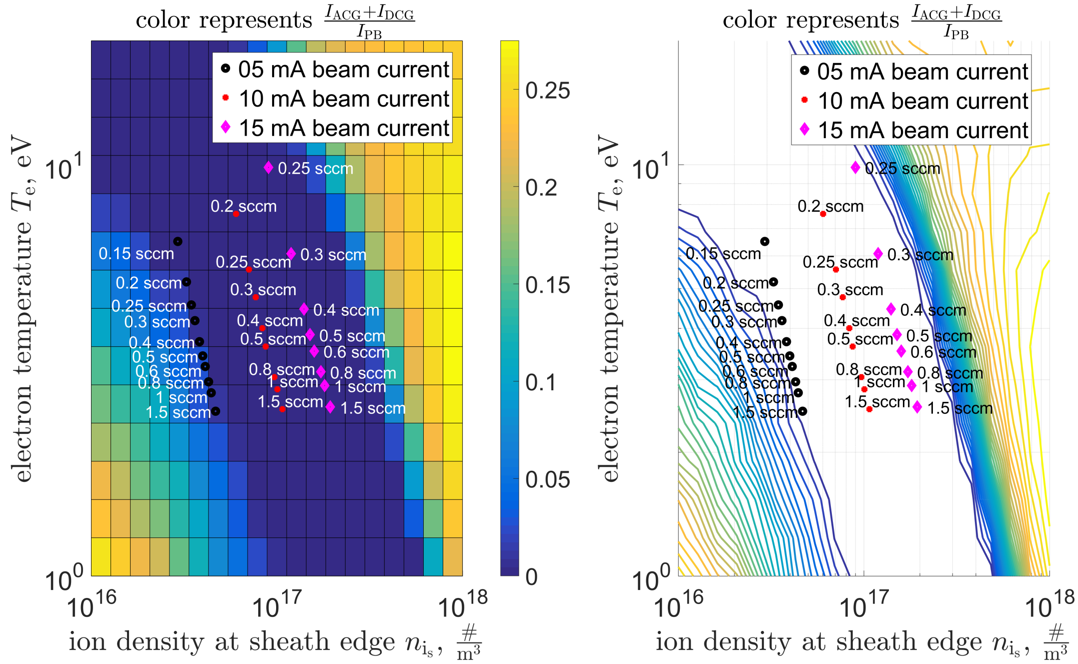

Figure 11. Sum of ratios for unwanted currents towards acceleration grid and deceleration grid respectively

E. Ion transmission coefficient

The ion transmission coefficient as illustrated in Fig. 12 also varies with changing ion beam current, but is rather independent of the inlet mass flow.

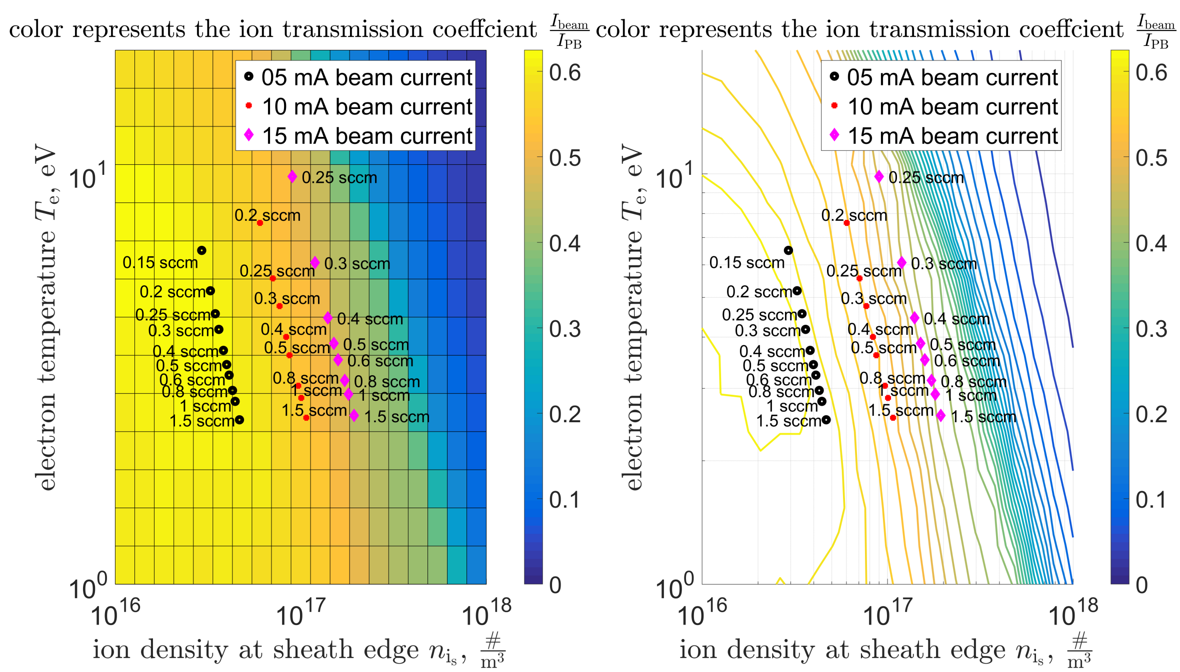

Figure 12. ion transmission coefficient

F. Thrust

The maximum possible thrust $\vec{F}_{\max}$ for a perfect non-divergent extraction is calculated by

$$\vec{F}_{\max} = \dot{m} v_{\mathrm{e}} = I_{\mathrm{b}} \frac{m_{\mathrm{i}}}{e} \sqrt{\frac{2}{m_{\mathrm{i}}} \left(\frac{1}{2} m_{\mathrm{i}} v_{\mathrm{b}}^2 + \Phi_{\mathrm{PB}} e \right)} \tag{11}$$

where $\dot{m}$ is the mass flow rate of exhaust and v_{e} is the exhaust velocity. This velocity is calculated based on the exhaust energy which is the sum of kinetic energy and potential energy. Both energies are known at the plasma boundary. As illustrated in Fig. 13 the thrust F_{x} is normalized by $F_{\max}$ to restrict the value range from 0 to 1. Note that an aperture with perfect symmetry and no alignment has been simulated. At this simulation the loss of thrust due to beam divergence is roughly 2 % for the worst operating point.

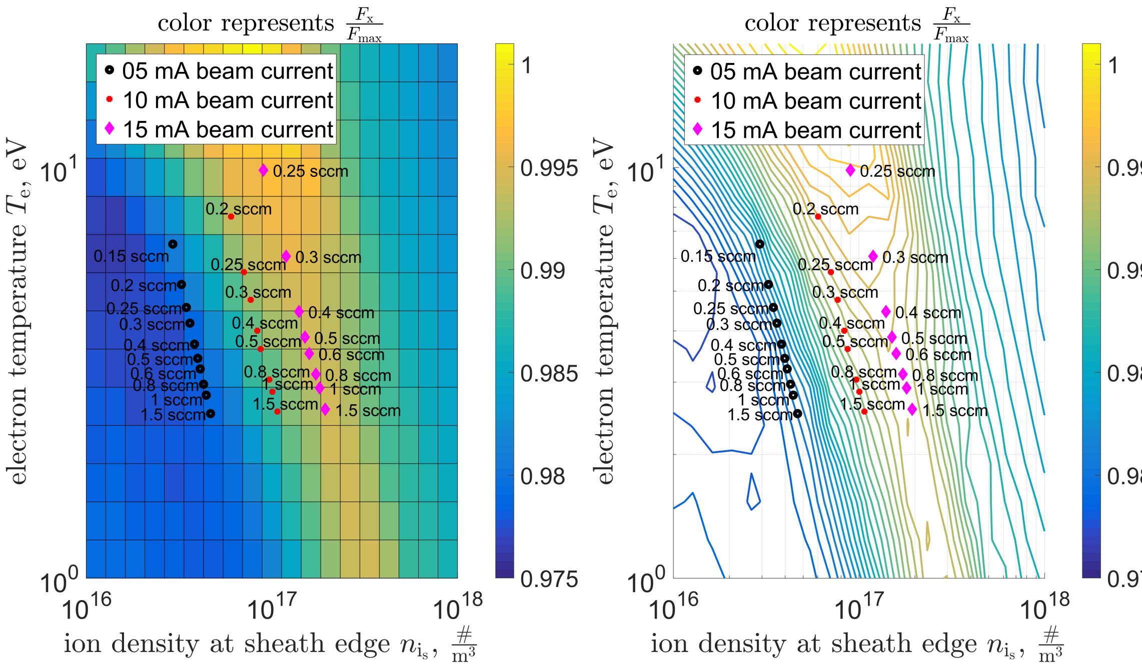

Figure 13. Thrust in x dimension, normalized

The proportions of the radial forces F_{y} and F_{z} to $F_{\max}$ are below $3 \cdot 10^{13}$ for every operating point. This coincides with our expectation. By simulating a symmetrical round aperture the radial forces cancel each other out.

The particle integration in our code can produce numerical errors which would disregard the energy conservation. To check for this error an additional summation is implemented which sums up the absolute values of all forces instead of using a vectorial summation. If the energy is conserved by the simulation the result has to agree with $F_{\max}$. In our simulations the deviation is below 0.35 % for every operating point.

IV. Conclusion

A 3D ion extraction code is developed to calculate the ion currents towards all extraction grids as well as the generated thrust. Our calculated trajectories are compared with the results of the established simulation software IGUN[10] and show good accordance. 300 simulations of the extraction code are carried out to characterize the grid behavior in dependence on ion sheath density and electron temperature. In accordance with Ref. 5, our simulations predict cross-over for low ion sheath density and direct impingement for high ion sheath density. Our code is coupled self-consistently with a thruster model. This allows us to examine, how the grid system behaves, if ion beam current and mass flow are changed.

Variation of the beam current influences the grid operating point. Cross-over, direct impingement and a change of the ion transmission coefficient are observed. A variation of the mass flow changes the plasma parameters, in particular, electron temperature and ion density. In our simulation runs we can observe that both changes cancels each other out. If the ion density decreases, the electron temperature will increase accordingly. The combination of both changes leads to a new grid operating point which has nearly the same ion transmission coefficient and grid currents as the previous one.

References

[1]Volkmar, C., Ricklefs, U., and Klar, P. J., "Self-Consistent Numerical 0D/3D Hybrid Modeling of Radio-Frequency Ion Thrusters," Trans. JSASS Aerospace Tech. Japan, Vol. 14, No. ists30, 2016, pp. 23-32.

[2]Volkmar, C., "Selbstkonsistente numerische 1D/3D Hybridmodellierung von Radiofrequenz-Ionentriebwerken", doctoral thesis, Justus-Liebig-Universitaet Giessen, Giessen, 2015.

[3]Dobkevicius, M., and Feili, D., "A coupled performance and thermal model for radio-frequency gridded ion thrusters," Eur. Phys. J. D, Vol. 70, No. 227, 01.11.2016

[4]Dobkevicius, M., and Feili, D., "Multiphysics Model for Radio-Frequency Gridded Ion Thruster Performance," JOURNAL OF PROPULSION AND POWER, Vol. 33, No. 4, JulyAugust 2017

[5]Goebel, D. M., and Katz, I., *Fundamentals of Electric Propulsion: Ion and Hall Thrusters*, 1st ed., Wiley, New Jersey, USA, 2008.

[6]Leiter, H. J., Entwicklung und physikalische Untersuchung eines Hochfrequenz-Ionentriebwerks unter besonderer Beruecksichtigung des Extraktionsgittersystems und der Ionisatorform, doctoral thesis Justus-Liebig-Universitaet Giessen, Giessen, 2000.

[7]Tartz, M., Peters J. H., and Neumann, H., "Grid performance models using Design of Experiments (DoE) methods," Proceedings of the 29th International Electric Propulsion Conference, Princeton University, 2005, Proceeding IEPC 2005-139.

[8]Goebel, D. M., Analytical Discharge Model for RF Ion Thrusters, IEEE Transactions on Plasma Science, Vol. 36, No. 5, 2008, pp. 2111-2121.

[9] Lieberman, M. A., and Lichtenberg, A. J., *Principles of Plasma Discharges and Materials Processing*, 2nd ed., Wiley, New Jersey, USA, 2005.

[10] Becker, R., and Herrmannsfeldt, W.B., IGUN-A program for simulation of positive ion extraction including magnetic fields, Review of Scientific Instruments, Vol. 63, No. 4, 1992, pp. 2757-2758.

[11] Kalvas, T., Tarvainen, O., Ropponen, T., Steczkiewicz, O., Aerje, J., and Clark, H., IBSIMU: A three-dimensional simulation software for charged particle opticsa), Review of Scientific Instruments, Vol. 81, No. 2, 2010.

[12] Kalvas, T., "DEVELOPMENT AND USE OF COMPUTATIONAL TOOLS FOR MODELLING NEGATIVE HYDROGEN ION SOURCE EXTRACTION SYSTEMS", doctoral thesis, University of Jyvaeskylae, Jyvaeskylae, 2013.

[13] Farnell, C. C., T., "PERFORMANCE AND LIFETIME SIMULATION OF ION THRUSTER OPTICS", doctoral thesis, Colorado State University, Fort Collins, 2007.

[14] Birdsall, C. K., and Langdon, A. B., *Plasma Physics via Computer Simulation*, 1st ed., Adam Hilger, Bristol, Philadelphia and New York, 1991.

[15] Tskhakaya, D., Matyash, K., Schneider, R., and Taccogna, F., The Particle-In-Cell Method, Contrib. Plasma Phys, Vol. 47, No. 8-9, 2007, pp. 573-594

[16] Boris, J.P., "RELATIVISTIC PLASMA SIMULATIONOPTIMIZATION OF A HYBRID CODE," *Proceeding of Fourth Conference on Numerical Simulations of Plasmas*, Naval Research Laboratory, Washington, D. C., 10.1970, pp. 3-67.

[17] Self, S. A., Exact Solution of the Collisionless Plasma-Sheath Equation, The Physics of Fluids, Vol. 6, No. 12, 04.1963, pp. 1762-1768.

[18] Evans, D. J., Parallel S.O.R. iterative methods, Parallel Computing, Vol. 1, No. 1, 08.1984, pp. 3-18.